ELSEVIER

Catalysis Today 49 (1999) 201–209

CATALYSIS TODAY

# Enhancement of acidity and paraselectivity by the silynation in pentasil zeolites

R.A. Shaikh*, S.G. Hegde, A.A. Behlekar, B.S. Rao

*Catalysis Division, National Chemical Laboratory, Pune-411 008, India*

**Abstract**

Silynation of ZSM-5 zeolite by CVD technique and its advantages are reported. Modification by this technique passivates the external surface and thereby reduces the non-selective surface reactions. Further, the Bronsted acid sites are increased with successive silynations at the cost of Lewis sites. With increasing silynation narrowing of pore mouth was observed which enhanced the paraselectivity in the ethylbenzene disproportionation reaction. The observations are based on the results of FT-IR, MAS–NMR, TPD of ammonia and catalytic test reactions. 

*Keywords:* CVD; ZSM-5; TEOS; Disproportionation; Paradiethylbenzene

## 1. Introduction

Shape selective property of zeolites find numerous applications in industrial catalytic processes in the manufacture of paradialkylbenzenes. They are produced by modified zeolites by a variety of reactions like alkylation [1–3], isomerization [4] disproportionation and transalkylation [5] of monoalkylbenzenes. Such modifications are obtained by incorporating oxides of phosphorous, magnesium and boron [1–4,6,7] crystal size variation [8] and silynation with silicon alkoxide [9]. These studies indicated that chemical vapour deposition (CVD) of silica on the surface of the catalyst is better than all other methods.

Niwa et al. [10,11] have extensively studied this method by using $Si(OCH_3)_4$ as silynating agent and later on, it was applied to other zeolites and oxide catalysts [12,13]. They have studied in detail the deposition mechanism and the structure of deposited $SiO_2$. As the silicon alkoxide is polyfunctional, silicon chains are formed uniformly on the surface rather than silica clusters. Moreover, silicon bonds are first preferentially formed on heteroatoms (e.g. on Al atoms). So, pore size reduction is more efficient on alumina rich zeolites, because on highly siliceous zeolites, siloxane bonds are formed epitaxially on silanol groups, which needs more silicon deposition to narrow the pore opening. It was also noted that silica deposits equivalently on silanol (Si–OH) as well as bridging hydroxyl groups [Si–(OH)–Al] of zeolites. Similarly, on pure $Al_2O_3$, all available Al–OH groups are covered by a monolayer of $SiO_2$ before the second layer starts growing. However, Hibino et al. [12] observed that some samples of H-ZSM-5 needed comparatively more amount of silica deposition to achieve the required shape selectivity. On detailed examination by XPS and $^{27}Al$ MAS–NMR studies, they detected octahedral extralattice aluminium species on the sur-

*Corresponding author.

0920-5861/99/$ – see front matter 
PII: S0920-5861(98)00425-8

face of such samples. It was argued that silica deposits first on all available Al–OH groups rather than on Si–OH groups identical to pure $Al_2O_3$ surface and then further deposition on Si–OH groups leads to reduction in pore mouth opening. In that case, Bronsted acidity on such zeolites should increase on CVD of $SiO_2$ by analogy to CVD of $SiO_2$ on pure $Al_2O_3$ contrary to reported results. The present study was undertaken to investigate this ambiguity. Samples of H-ZSM-5 zeolites were modified by CVD of $SiO_2$, and acidity and shape selectivity of modified samples were studied through FT-IR, MAS–NMR and catalytic test reactions.

## 2. Experimental

Samples of pure H-ZSM-5 ($S_0$) were prepared as per the procedure described earlier [14]. For CVD of $SiO_2$, 12 g of zeolite sample was activated at 673 K in flowing nitrogen gas and exposed to vapours of silynating feed (10 ml $h^{-1}$) containing 50% toluene+45% methanol+5% tetraethyl orthosilicate (TEOS) at 473–483 K. The amount of silynation was controlled by controlling the time of contact of silynating agent. Concentration of TEOS in silynating feed and downstream condensate was monitored by gas chromatographic analysis on Shimadzu 15A model GC using SE-30 10% on Chromosorb W, 5 m, long stainless steel column at 373 K with thermal conductivity detector (TCD). The amount of silica deposited was calculated from the amount of reacted TEOS. After the required amount of TEOS was reacted, the sample was slowly flushed with a small flow of nitrogen progressively enriched with oxygen for 4–16 h depending on the amount of this reaction. In this manner, the organic residue (ethyl groups) on the surface was oxidatively decomposed and removed. The procedure was repeated for higher $SiO_2$ deposition. In this way, samples were obtained which contained various amounts of silica deposited (1.8%, 4.6%, 7.6%, 9.8% and 12.5%). Catalytic data was obtained by ethylbenzene disproportionation in a downflow integral silica reactor as discussed earlier [15]. The product was analysed by gas chromatography using modified column reported in thesis [15] at 373 K and nitrogen as carrier gas with flame ionization detector (FID).

FT-IR spectra (Nicolet 60SXB, 2 $cm^{-1}$ resolution) were recorded in transmittance mode using self-supporting pressed discs (5–6 mg $cm^{-2}$). The sample was activated in situ in a homemade sample cell at 673 K in vacuum ($10^{-6}$ Torr) for 6 h and then cooled to 373 K before recording the spectra. For acidity determination, the activated sample was exposed to pyridine vapour (10 mm) at 393 K for 30 min, then physically adsorbed pyridine was removed by evacuation and the spectrum was recorded. Then, pyridine was successively desorbed from the sample by evacuating at 473, 523, 573, 623 and 673 K, cooled to 373 K every time and the spectra were recorded. The signal was averaged over 1000 scans before recording spectra in every case. The solid state MAS–NMR $^{29}Si$ and $^{27}Al$ was recorded at 295 K (Bruker MSL-300 FT-NMR) using TMS and aqueous aluminium chloride solution as standard, respectively. For acetyl acetone treatment, the sample was activated in vacuum ($10^{-5}$ Torr) at 673 K, and then cooled in situ before contacting with ethanolic solution of 10% (w/w) of acetyl acetone for 4 h. Excess solution was removed by evacuation at 295 K before recording $^{27}Al$ MAS–NMR spectra immediately.

The crystallinity of zeolites was determined by X-ray diffraction (XRD), scanning electron microscopy (SEM) and the surface area was determined by nitrogen adsorption (Omnisorb). Chemical analysis was carried out by X-ray florescence (XRF).

## 3. Results and discussion

### 3.1. Crystallinity

SEM and X-ray diffraction results revealed that silynation treatment does not alter the morphology and crystallinity of the samples. Chemical composition, amount of silica deposited, and acid strength distribution obtained from TPD for samples $S_0$–$S_{05}$, $S_*$, and $S_{*1}$ are presented in Table 1.

### 3.2. Silica deposition

Deposition of silica occurs readily at 493 K on $S_*$ and $S_0$ samples as reported previously [12]. The amount of deposition was systematically varied keeping in view to modify the surface character gradually.

Table 1
Chemical composition of H-ZSM-5 (260), unit cell: $Na_{0.04}[(SiO_2)_{95.27}(Al_2O_3)_{0.73}]\cdot 11H_2O$

| No. | Name | Description | Amount of desorbed $NH_3$ on different sites | | |
|---|---|---|---|---|---|
| | | | Weak | Medium | Strong |
| 1 | $S_0$ | H-ZSM-5 ($SiO_2/Al_2O_3$=260) | 1.20 | 0.90 | 0.75 |
| 2 | $S_{01}$ | Silynated $S_0$ (1.8% $SiO_2$) | 1.25 | 0.95 | 0.80 |
| 3 | $S_{02}$ | Silynated $S_{01}$ (4.62% $SiO_2$) | 1.35 | 1.00 | 0.84 |
| 4 | $S_{03}$ | Silynated $S_{02}$ (5.63% $SiO_2$) | 1.39 | 1.20 | 0.87 |
| 5 | $S_{04}$ | Silynated $S_{03}$ (9.86% $SiO_2$) | 1.50 | 1.30 | 0.92 |
| 6 | $S_{05}$ | Silynated $S_{04}$ (12.56% $SiO_2$) | 1.40 | 0.93 | 0.83 |
| 7 | $S_*$ | $S_0$ steam treated for 4 h at 923 K | 0.95 | 0.63 | 0.60 |
| 8 | $S_{*1}$ | Silynated $S_{*1}$ (1.9% $SiO_2$) | 0.70 | 0.60 | 0.40 |

Accordingly, silynation was discontinued at 1.85% for the samples $S_{*1}$ and $S_{01}$, whereas for $S_{02}$ and $S_{03}$ it had to be done twice with intermediate activation. For samples $S_{04}$ and $S_{05}$ to achieve the required amount of silynation, the procedure has to be repeated three times. In this fashion, 1.8%, 1.9%, 4.62%, 7.56%, 9.86% and 12.52% of silica was deposited on $S_{*1}$ and $S_{01}$–$S_{05}$, respectively. It is observed that the accumulated silica in each deposition cycle decreased as the number of cycles of silynation increases.

The scanning electron microscope (SEM, Fig. 1) does not show any silica accumulation on the surface for samples $S_{01}$–$S_{03}$. The sample $S_{04}$ showed few aggregates of tiny particles grown on the large crystal surface. $S_{05}$ samples clearly showed a typical nature of silica being accumulated like debris on the external surface.

### 3.3. MAS–NMR studies

MAS–NMR of $^{29}Si$ and $^{27}Al$ observation gives information on (i) the difference between Si coordination to other atoms and to various Al atoms and (ii) the difference between Al tetrahedrally and octahedrally coordinated to oxygen atoms [16]. The $^{27}Al$ MAS–NMR provides the only satisfactory method to distinguish between Al in the framework and the extraframework sites. Zeolite samples which were dealuminated are known to have ''NMR invisible'' aluminium species [17–20]. On impregnation with acetyl acetone, these invisible aluminium species become visible octahedral aluminium acetonate species [21–23]. In the $^{27}Al$ MAS–NMR spectrum of sample $S_*$ and $S_{*1}$ (Fig. 2, curve a and b), the initial ratio of tetrahedral aluminium at 50 ppm and octahedral aluminium at 1 ppm does not change significantly on acetyl acetone treatment. For samples $S_{01}$–$S_{04}$ also, this ratio decreased gradually. The acetyl acetone treatment had no influence on $^{27}Al$ NMR spectra of $S_{*1}$ sample (not shown). These imply that on CVD of $SiO_2$, invisible tetrahedral aluminium species decreases in amount until it completely vanished for the $S_{04}$ sample. These effects are further investigated by TPD of ammonia and FT-IR spectroscopic measurements.

### 3.4. TPD of ammonia

Acid strength distribution can be derived from the rate of desorption of chemisorbed ammonia at increasing temperatures. Three distinct stages for desorption of ammonia at 333–373 K, 423–553 K and 573–773 K were observed (Fig. 3) corresponding to weak, medium and strong acid sites, respectively. The amount of chemisorbed ammonia at 298 K is presented in Table 1. On silynation, the pattern of acid strength distribution is altered as can be seen by the not so well-resolved peaks in the TPD curves. However, the total amount of chemisorbed ammonia increases as the silynation increased from 1.8% to 12.2% for samples $S_0$–$S_{05}$. It should be noticed that for sample $S_{05}$, the quantity of chemisorbed ammonia indicates that the internal acidity is maintained even if excessive silynation has taken place, wherein pyridine adsorption experiment in IR indicates lower acidity. It is due to excessive pore narrowing which hinders the adsorption of pyridine into the internal acid sites of $S_{05}$.

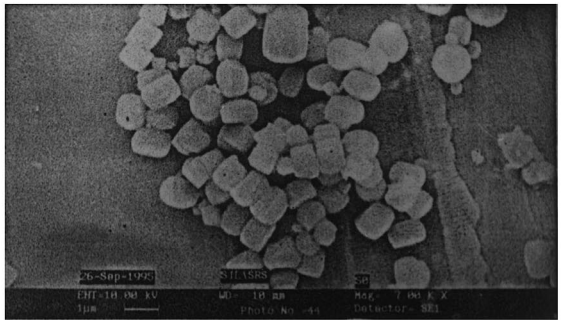

(A)

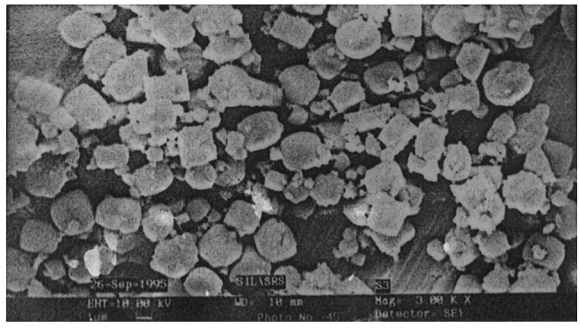

(B)

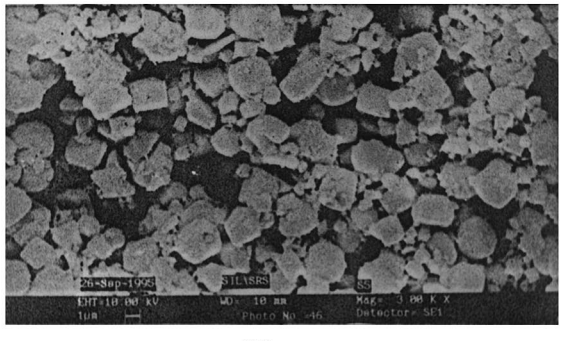

(C)

Fig. 1. SEM photographs of (A) $S_0$, (B) $S_3$, (C) $S_5$.

### 3.5. FT-IR spectra

*Hydroxyl groups*. The acidic properties of H-ZSM-5 samples $S_*$ and $S_0$ before and after silynation were studied by FT-IR methods. In the region of –O–H, stretching vibration bands (Fig. 4, $S_0$-$S_5$) are observed at 3736, 3700, 3676, 3607 and 3490 $cm^{-1}$ for $S_*$ and $S_0$ samples. These bands are assigned to isolated

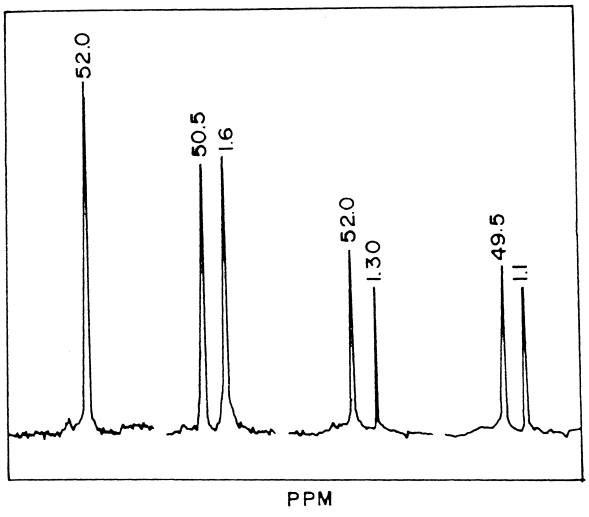


Fig. 2. Masnmr.

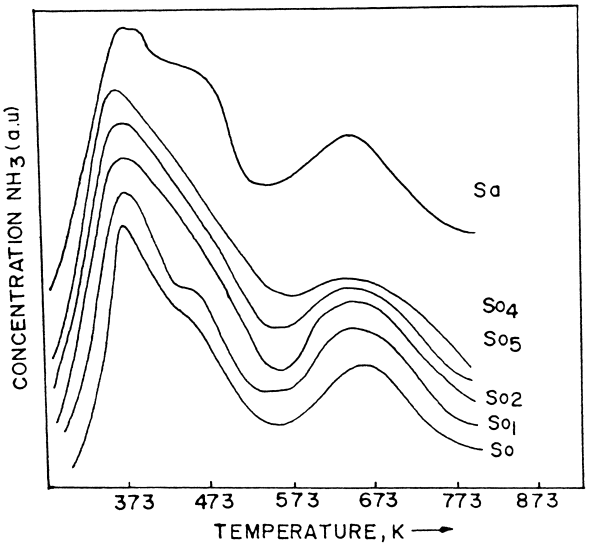


Fig. 3. TPD of ammonia.

silanol groups, extralattice silica–alumina species, bridging hydroxyl and hydrogen bonded hydroxyl groups, respectively. The band due to extraneous silica–alumina (3676 $cm^{-1}$) is not visible distinctly in the spectra of $S_*$, instead somewhat broad band is observed at 3682 $cm^{-1}$ which is attributed to silica–alumina debris in the sample. It should be noted that for sample $S_*$, octahedral Al species (1 ppm) are observed in MAS–NMR and the sample $S_0$ does not

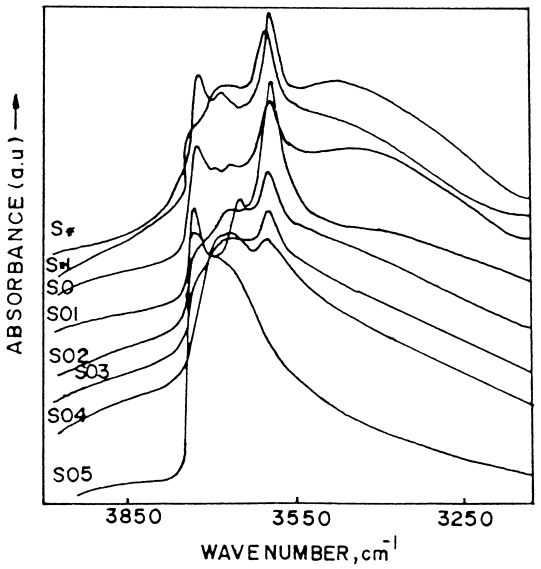


Fig. 4. FTIR hydroxyl groups.

show octahedral species. It is suggested [24] that these species are similar to the activated sites of amorphous silica–alumina catalyst. Deposition of 1.8% of $SiO_2$ (sample $S_{01}$) shows a decrease in band intensity at 3736, 3700, 3676 and 3490 $cm^{-1}$, and a clear band at 3655 $cm^{-1}$ appears. This clearly shows that initial $SiO_2$ deposition results in a decrease in (i) isolated and hydrogen bonded silanol groups and (ii) silica–alumina extralattice species. It implies that silynated samples has less defect sites, and less extralattice silica–alumina species probably due to the structure healing effect of CVD of $SiO_2$. However at this stage, FT-IR still indicates the presence of some extralattice aluminium species, and a band at 3655 $cm^{-1}$. On further silynation of 4.6%, 7.6%, 9.9%, and 12.5% for samples $S_{02}$–$S_{05}$, a broad band with a peak at 3690 $cm^{-1}$ in the region of 3750–3200 $cm^{-1}$ progressively overlaps with all types of surface hydroxyl groups originally present. In the spectrum of any silica, the hydroxyl region consists of two components: (i) a sharp band at 3740 $cm^{-1}$ corresponding to isolated hydroxyls and (ii) a broad band in the region 3700–3200 $cm^{-1}$ which is due to hydrogen bonded hydroxyl groups. The peak position of the latter entirely depends upon the amount of hydrogen bonding. Shrinivasan et al. [25] have compared IR spectra of cabosil derived from $SiCl_4$, Degussa Aerosil-972

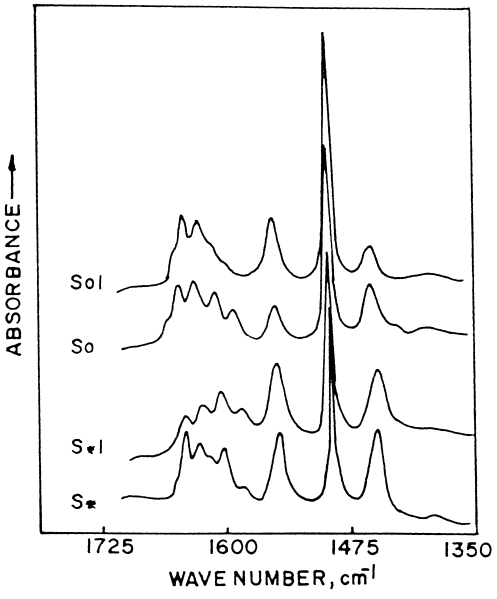


Fig. 5. IR-spectra of adsorbed pyridine.

obtained from dimethyl cholorosilane, Stober silica obtained from TEOS and acid washed Davison-952 silica gel. They reported that Cabosil and Davison both show isolated and hydrogen bonded hydroxyl groups, whereas Degussa and Stober show only hydrogen bonded silanol groups. Overlayers of silica derived from CVD of TEOS on $S_0$ sample are identical to those of Stober silica obtained from TEOS. IR spectra of silynated $S_*$ samples $S_{*1}$ are remarkably different (Fig. 5). Even in the initial stage of silynation with 1.8% of $SiO_2$, intensity of all bands except the bridging hydroxyl have increased. The nature of IR spectra of $S_{*1}$ samples further silynated, however, are similar to those of silynated $S_0$ samples. Takashi, Hibino et al. [12] and Niwa et al. [11] have extensively studied the mechanism of CVD of $SiO_2$ on zeolites and proposed that protruded $SiO_2$ is deposited as layer by layer producing pure silica surface with vicinal silanol groups. Such silanol groups can mutually interact by hydrogen bonding to produce a broad absorption band in the region of 3700–3200 $cm^{-1}$.

### 3.6. Pyridine adsorption

In the (Fig. 4) pyridine absorption bands on $S_*$, $S_{*1}$, $S_0$ and $S_{01}$ at 373 K are depicted. Pyridine adsorption leads to the formation of pyridinium ion (1632, 1490 and 1545 $cm^{-1}$) coordinated species (1620, 1490 and 1455 $cm^{-1}$). Relative amount of Bronsted and Lewis acid sites as a function of temperature of evacuation for parent and silynated samples are presented in Table 2.

From Table 2, the following features are notable.

1. Parent sample $S_0$ has more Bronsted acid sites and less Lewis acid sites as compared to sample $S_*$.
2. On silynation, Bronsted acid sites of $S_0$ increased significantly at the cost of Lewis acid sites, whereas for $S_*$ Bronsted acid sites decreased comparatively (decrease in the relative acid strength of Lewis sites and increase in the relative Bronsted acid sites for samples $S_0$–$S_{05}$).

Table 2
Relative acid strength distribution

| S | Temperature (K) of chemisorption | | | | | | | | | | | | | |
|---|---|---|---|---|---|---|---|---|---|---|---|---|---|---|
| | 373 | | 423 | | 473 | | 523 | | 573 | | 623 | | 673 | |
| | B | L | B | L | B | L | B | L | B | L | B | L | B | L |
| $S_0$ | 0.61 | 0.45 | 0.57 | 0.31 | 0.41 | 0.23 | 0.27 | 0.12 | 0.16 | 0.10 | 0.07 | 0.04 | 0.04 | 0.02 |
| $S_{01}$ | 0.75 | 0.37 | 0.64 | 0.27 | 0.49 | 0.19 | 0.32 | 0.14 | 0.21 | 0.06 | 0.12 | 0.03 | 0.06 | 0.01 |
| $S_{02}$ | 0.78 | 0.36 | 0.67 | 0.24 | 0.56 | 0.14 | 0.38 | 0.08 | 0.27 | 0.04 | 0.19 | 0.02 | 0.07 | 0.01 |
| $S_{03}$ | 0.84 | 0.35 | 0.70 | 0.21 | 0.60 | 0.11 | 0.46 | 0.05 | 0.32 | 0.02 | 0.21 | 0.01 | 0.08 | 0.01 |
| $S_{04}$ | 0.90 | 0.33 | 0.73 | 0.19 | 0.65 | 0.05 | 0.51 | 0.02 | 0.35 | 0.01 | 0.22 | – | 0.09 | – |
| $S_{05}$ | 0.27 | 0.23 | 0.15 | 0.07 | 0.09 | 0.03 | 0.05 | 0.01 | 0.05 | – | 0.04 | – | 0.04 | – |
| $S_*$ | 0.53 | 0.60 | 0.44 | 0.50 | 0.35 | 0.35 | 0.27 | 0.22 | 0.19 | 0.15 | 0.10 | 0.13 | 0.05 | 0.10 |
| $S_{*1}$ | 0.49 | 0.56 | 0.42 | 0.45 | 0.32 | 0.35 | 0.22 | 0.21 | 0.15 | 0.14 | 0.09 | 0.08 | 0.05 | 0.05 |

S: Sample; B: Bronsted acid sites/g; L: Lewis acid sites/g.

In order to analyse and understand the above results on CVD of $SiO_2$ on H-ZSM-5 zeolite samples we have to consider that:

1. CVD of $SiO_2$ commences preferentially on heteroatoms on surface OH groups.
2. TEOS being neutral, preferentially reacts with relatively basic sites on the surfaces like alumina species.
3. Monolayer coverage completes before the second layer starts to grow.
4. Silica monolayer on alumina surface can produce weak Bronsted acid sites similar to zeolitic acid sites.
5. ''NMR invisible'' aluminium species in zeolites are probably dealuminated species still attached to one or two points of the lattice.
6. Dealuminated zeolite samples show surface enrichment of aluminium species.

CVD of silica on the external surface of zeolite is known to passivate the external surface acidity, and the total acidity should decrease correspondingly, whereas we observe that it is true only for samples showing octrahedral aluminium species and no ''NMR invisible'' tetrahedral aluminium species (e.g. sample $S_{*1}$). On the contrary, samples showing no octrahederal and considerable ''NMR invisible'' aluminium species (e.g. $S_{01}$) show significant increase in Bronsted acidity and decrease in Lewis acidity. Considering salient features of silynation described previously, aluminium of the surface species are the active centres for initial silynation. When such aluminium species are ''NMR invisible'' deposited silica can easily bridge them back to the lattice. This is how reinsertion of alumina to the lattice can take place. The moderate hydrothermal environment of the gaseous phase of silynation should be a sufficiently favourable condition for such a structure healing process. This seems to be the probable reason for the increase in Bronsted acidity and the decrease in Lewis acidity on silynation of $S_0$ sample. Aluminium species in $S_*$ sample is probably in the form of silica–alumina dense phase debris, which could not be inserted into the lattice by silynation.

### 3.7. Catalytic activity

Toluene disproportionation using zeolite catalysts [28] and decomposition of ethylbenzene over highly dealuminated Zeolite Y [29] were reported in literature. Ethylbenzene can react over HZSM-5 zeolites mainly as shown in Scheme 1.

Results of ethylbenzene disproportionation over the silynated samples is presented in Table 3. Earlier reports on these type of reactions [28,29] indicated selectivity of 40–50% to paradialkylbenzenes. From

Table 3
Ethylbenzene disproportionation over silynated samples

| Sample | $S_0$ | $S_{01}$ | $S_{02}$ | $S_{03}$ | $S_{04}$ | $S_{05}$ |
|---|---|---|---|---|---|---|
| Amount of $SiO_2$ | 00.00 | 01.80 | 04.62 | 07.56 | 09.86 | 12.52 |
| Product distribution (wt%) | | | | | | |
| Non-aromatics | 00.12 | 00.70 | 00.58 | 00.43 | 00.34 | 00.08 |
| Benzene | 17.09 | 15.30 | 15.03 | 13.60 | 13.45 | 09.08 |
| Toluene | 01.10 | 01.72 | 00.83 | 01.24 | 01.19 | 00.45 |
| Ethylbenzene | 62.68 | 64.60 | 67.02 | 69.64 | 70.69 | 79.42 |
| $\sum$Xylene | 00.28 | 00.13 | 00.05 | 00.03 | 00.02 | – |
| $\sum C_9$ aromatics | 00.99 | 01.78 | 01.84 | 01.11 | 00.97 | 00.19 |
| *m*-Diethylbenzene | 09.55 | 04.75 | 03.02 | 00.64 | 00.01 | 00.10 |
| *p*-Diethylbenzene | 05.85 | 10.27 | 10.80 | 12.58 | 12.67 | 10.61 |
| $\sum$Diethylbenzene | 15.40 | 15.02 | 13.82 | 13.22 | 12.68 | 10.71 |
| $\sum$High boil. frac. | 02.34 | 00.75 | 00.83 | 00.73 | 00.66 | 00.07 |
| Benz/$\sum$Diethylbenzene | 01.91 | 01.75 | 01.87 | 01.77 | 01.80 | 01.46 |
| $Sel._{p\text{-diethylbenzene}}$ | 38.00 | 68.40 | 78.10 | 95.10 | 99.90 | 99.80 |
| $Sel._{\text{ethylbenzene}\rightarrow\sum\text{diethylbenzene}}$ | 41.30 | 42.40 | 41.90 | 43.50 | 43.30 | 52.00 |
| Conv. ($\alpha$) ethylbenzene | 37.30 | 35.40 | 33.00 | 30.40 | 29.30 | 20.60 |

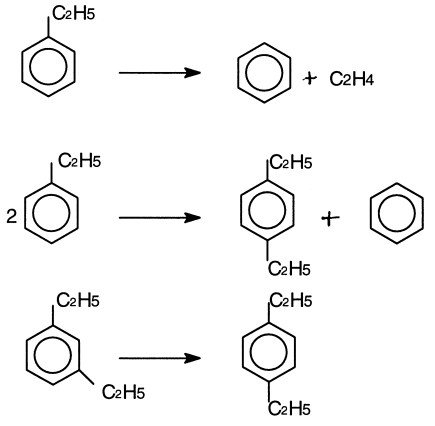


Scheme 1.

the results of the present study, we can see that concentration of benzene in product decreases from 17.1% to 13.4% for samples $S_{01}$–$S_{04}$. Benzene can originate from dealkylation as well as disproportionation of ethylbenzene. Dealkylation reaction requires stronger acid sites than disproportionation. It is reported that mildly dealuminated H-ZSM-5 having ''NMR invisible'' aluminium species is highly acidic due to the inductive effect of Lewis acid sites on Bronsted acid sites. As the Lewis acidity decreases on $SiO_2$ deposition, the influence of this Bronsted–Lewis acid pair should decrease. Consequently, dealkylation reaction should decrease preferentially, resulting in a decrease in benzene concentration. We should also note that ethylbenzene conversion drops from 37.3% to 29.3% for sample $S_0$–$S_{04}$ which can be mainly due to the decrease in dealkylation reaction, rather than the decrease in disproportionation. We should also note that dealkylation to disproportionation ratio drops from 1.9 to 1.4. It is in accordance with our acidity results (Table 2), wherein we have noticed an increase in Bronsted acidity and a decrease in Lewis acidity.

The most important effect of silynation is the remarkable enhancement of paraselectivity for diethylbenzene which goes from 38.0% to 99.9%. However, conversion in the case of $S_{05}$ drops down to 20.6% probably because of excessive silica deposition on pore opening causing diffusional constraints. It is in accordance with our pyridine adsorption results wherein Bronsted and Lewis acidity was considerably less because of poor accessibility of pyridine molecule to internal acid sites, but there is no decrease in the concentration of bridging hydroxyls groups, as determined by chemisorbed ammonia (TPD).

### 3.8. Mechanism of silynation

A schematic of the ZSM-5 catalyst surface structure can be represented [26] as shown in Fig. 6. Totally,

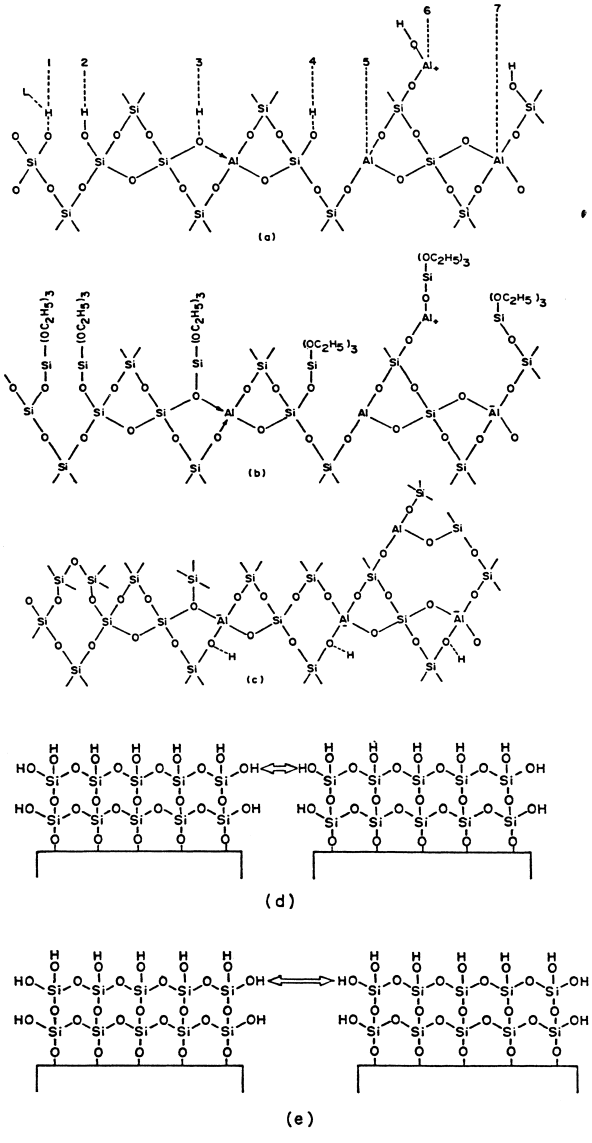


Fig. 6. (d) C.V.D. of $SiO_2$ protruding over pore month. (e) C.V.D. of $SiO_2$ epitaxially on surface.

seven types of acid sites are identified (Fig. 6(a)). During silynation, these groups are primarily regarded as target surface groups. When a feed consisting of toluene, methanol and TEOS is used, methanol converts to dimethyl ether and water on acidic sites as reported by Ono et al. [27]:

$$2CH_3OH \rightarrow CH_3OCH_3 + H_2O,$$

$$nCH_3OH \rightarrow \text{Hydrocarbons} + nH_2O.$$

The water molecules then hydrolyse TEOS partially producing hydroxy trimethoxysilane [HO $SiO(OCH_3)$], which adsorbed on the surface first on the exposed Al sites and then on hydroxyl nests as shown in Fig. 6(b). After calcination, the structure is getting healed by forming Al (Si)–O–Si bonds and a layer of $SiO_2$ is formed as shown in Fig. 6(c). Bonding occurs across the extralattice aluminium species, framework silanol groups and across the hydroxyl nests. Therefore, Bronsted acidity increases and Lewis acidity decreases simultaneously. Pore size reduction is taking place easily on less silicious surfaces like in Fig. 6(d) compared to that in Fig. 6(e) which is more silicious.

## 4. Conclusions

Our results prove for the first time that the CVD of $SiO_2$ on H-ZSM-5 zeolite showing ''NMR invisible'' aluminium species leads to an increase in Bronsted acid sites and a decrease in Lewis acid sites, no such changes take place for samples excessively dealuminated. It is proposed that aluminium species is in partially dealuminated state but is still attached to the framework by one or two points and get reinserted totally into the framework positions by silynation. They are then covered by deposited silica extra layers and result in internal Bronsted acid sites. Such catalysts become highly paraselective without losing in activity due to the alteration in pore mouth opening. $SiO_2$ deposition can also passivate the external surface acidity.

## References

[1] G. Mirth, J.A. Lercher, J. Catal. 147 (1994) 199.
[2] T. Hibino, M. Niwa, Y. Murakami, J. Catal. 128 (1991) 551.
[3] W.W. Kaeding, J. Catal. 95 (1986) 512.
[4] D.H. Olson, W.O. Haag, in: T.E. Whytes Jr. (Ed.), Catalytic Materials, ACS Symposium Series, vol. 248, ACS, Washington, DC, 1984, p. 257.
[5] J. Das, Y.S. Bhat, A.B. Halgeri, Catal. Lett. 20 (1993) 349.
[6] J.H. Kim, S. Namba, T. Yashima, Bull. Chem. Soc. Jpn. 61 (1988) 1051.
[7] W.W. Kaeding, C. Chu, L.B. Young, S.A. Butter, J. Catal. 69 (1981) 392.
[8] G. Paparatto, T. Moreitti, G. Leoprti, T. Gattes, J. Catal. 105 (1987) 227.
[9] J.H. Kim, A. Ishida, M. Okijima, M. Niwa, J. Catal. 161 (1996) 387.
[10] M. Niwa, N. Katada, Y. Murakami, J. Catal. 134 (1992) 340.
[11] M. Niwa, N. Katada, T. Murakami, J. Phys. Chem. 94 (1990) 6441.
[12] T. Hibino, M. Niwa, T. Murakami, Zeolites 13 (1993) 518.
[13] Y. Chu, Y. Chen, A.Z. Yan, Q.H. Xu, in: J. Weitkamp (Ed.), Studies in Surface Science and Catalysis, vol. 84, Elsevier, Amsterdam, 1994, p. 1035.
[14] R.J. Argauer, G.R. Landolt, US Patent 3 702 886 (1972).
[15] R.A. Shaikh, Shape selective catalysis over modified zeolites, Ph.D. Thesis, 1995.
[16] G. Engelhardt, D. Mechel, in: High Resolution Solid State NMR of Silicates and Zeolites, Wiley, New York, 1987.
[17] S.M. Alexander, D.M. Bibby, R.F. Howe, R.H. Meinhold, Zeolites 13 (1993) 441.
[18] J. Klinowski, J.M. Thomas, C.A. Fyfe, G.C. Gobbi, Nature 296 (1982) 533.
[19] E. Brunner, H. Ernst, D. Freude, M. Hunger, H. Pfiefer, in: P.J. Gorbet (Ed.), Innovation Zeolite Material Science, Elsevier, Amsterdam, 1988, p. 155.
[20] J. Klinowski, C.C. Fyfe, G.C. Gobbi, J. Chem. Soc. Faraday Trans. 1 81 (1985) 3003.
[21] V. Bosacik, D. Freude, T. Frohlich, H. Pfiefer, H. Schniedd, J. Call. Int. Sci. 85 (1982) 502.
[22] D. Freude, T. Frohlich, H. Pfeifer, G. Scheler, Zeolites 3 (1983) 171.
[23] J. Sonz, V. Fornes, A. Corma, J. Chem. Soc. Faraday Trans. 1 84 (1988) 3113.
[24] D. Barthomeuf, Zeolites 10 (1990) 131.
[25] S. Shrinivasan, A.K. Datye, M.H. Smith, C.H.F. Peden, J. Catal. 145 (1994) 565.
[26] M.B. Sayed, R.A. Kyad, R.P. Cooney, J. Catal. 88 (1984) 137.
[27] Y. Ono, E. Inui, T. Mori, Z. Phys. Chem. (N.F.) 115 (1979) 99.
[28] J.A. Amelse, Stud. Surf. Sci. Catal. 33 (1988) 165.
[29] E.V. Sobrinho, D. Cardose, E. Fulabellas-Aguir, J.G. Silva, Appl. Catal. A 127 (1995) 157.